Academic Journal of Engineering and Technology Science
ISSN 2616-5767 Vol.3, Issue 6: 199-208, DOI: 10.25236/AJETS.2020.030620

Prediction on Transient Thermal Performance of Heat Pipe Array for a Battery Thermal Management

Chaoyi Wan

Jiangsu University of Technology, Changzhou, 213001, China

ABSTRACT. *By using the method of transient numerical calculation, the effects of different coolant flow rates, coolant inlet temperature and input power on the thermal performance of the heat pipe cooling system are studied. Results shows temperature increased with the input power and coolant inlet temperature and decreased with the increasing coolant flow rate, and the temperature difference of the battery surface also increased with the input power and decreased with the increasing coolant flow rate. Within the scope of this study when coolant inlet temperature is 15℃ the maximum temperature is always below 40 ° C .*

KEYWORDS: *Thermal management, Heat pipe, Numerical model, Transient thermal performance*

1. Introduction

Lithium-ion battery is the promising energy storage equipment for electric vehicles and hybrid electric vehicles for its high energy density [1, 2]. The optimum working temperature of the lithium battery is 25 °C -40 °C [3-6], the maximum temperature difference should not exceed 5 °C in one battery pack [7, 8]; otherwise, it may cause serious safety problems [6, 7]. The heat pipe cooling system which uses liquid-gas phase change without consuming extra power has become the most promising cooling method in lithium-ion battery thermal management system with excellent heat transfer performance and rapid response capability [3, 4, 9, 10].

The power battery generates heat more than 50 W [11, 12], and more during acceleration and other high charging or discharging conditions. Rao et al. [4] conducted experimental research which shows that the maximum temperature of the battery surface can be controlled below 50 °C when heat generation of the battery is less than 50 W. However, the maximum temperature difference is about 8 °C. The heat load should not exceed 30 W to maintain the surface temperature difference within 5 °C. The experiment studied of Wang et al. [13] pointed out that the battery temperature can stay below 70 °C when the heat generation per cell is between 20-40 W. Or the amount of heat generation cannot exceed 10 W in order to the maximum temperature below 40 °C. Ye et al.[14] experimentally studied different

ISSN 2616-5767 Vol.3, Issue 6: 199-208, DOI: 10.25236/AJETS.2020.030620

cooling strategies. The result shows that the cooling strategy with a lag time between the start-up of HP-BTMS and battery is helpful to improve the thermal performance of HP-BTMS.

2. Numerical Setup

2.1 Geometry Models and Simplifications

Fig. 1 shows a configuration of the heat pipe cooling system for a prismatic battery pack. Between two prismatic batteries ($118mm \times 63mm \times 13mm$) sandwiched evaporator sections of four heat pipes. The heat generated in the battery is transferred to the condenser section through the heat pipe and then emitted into the coolant flow through the cooling passage ($300mm \times 60mm \times 12mm$). Each heat pipe were flattened from tubular condenser (Φ=6.0mm) to rectangular evaporator section ($2.0mm \times 8.5mm$). Cross section radius of vapor core is 0.002m. The total length of the heat pipe is 0.198m. Porosity of the wick region is 0.50. The copper cooling system is designed as similar as the heat pipe cooling system except that the heat pipes are turned to pure copper rods.

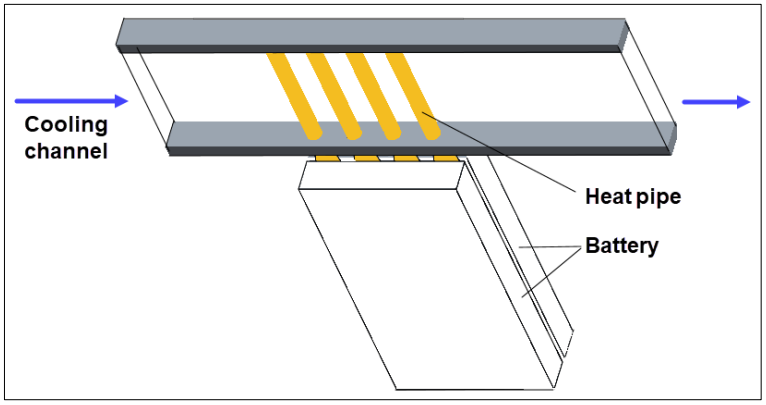

Fig.1 The Configuration of the Heat Pipe Cooling System for a Prismatic Battery Pack

It is complex and time-consuming to model all details for a battery pack cooled by heat pipe for phase changes and other phenomena in heat pipe. Even in the case of simulating one heat pipe, high computational resources are necessitated to characterize the mass and heat transfer during transient charging or discharging of the cell. Thus, one more efficient approach for numerical computation is adopted. The thermal behavior of a heat pipe on battery cooling would be treated as a thermal network of various components, and then the transient behavior can be described by first order linear ordinary differential equations [15]. Additionally, solving

ISSN 2616-5767 Vol.3, Issue 6: 199-208, DOI: 10.25236/AJETS.2020.030620

electro-chemical reactions of a battery is also too complicated for only presenting the thermal behavior of battery cell (multi-layer structure). Therefore, a simplified model without considering electro-chemical reactions is applied to present the heat generation of the battery, as well as the thermal properties of a multi-layered battery cell. This approach is well validated by comparisons with experimental and numerical studies and is applied in many pieces of literature [1, 9, 11, 15].

2.2 Model Formulation of the Heat Pipe

2.2.1. Copper Shell

The thermal properties of copper were applied directly to the copper shell during this simulation because the heat transfer through the copper shell of the heat pipe is entirely conduction.

2.2.2. Wick Region

In the present study, a heat pipe with a higher maximum heat transfer limit than the target heat load has been selected to avoid drying during operation. The wick region was considered as a porous structure filled with water. A widely accepted model developed by Chi et al. [16] can be used to calculate the effective thermal conductivity of the wick region k_{wick}:

$$k_{wick} = \frac{k_l[(k_l + k_s) - (1-\varepsilon)(k_l - k_s)]}{[(k_l + k_s) + (1-\varepsilon)(k_l - k_s)]} \quad (1)$$

where k_l and k_s are respectively the thermal conductivity of working fluid and sintered copper powder porous wick, and ε is the porosity. In this study, the effective thermal conductivity of the wick region was calculated to be 1.814 $Wm^{-1}K^{-1}$.

The volumetric averaged density of the mixture of water and sintered copper powder porous wick could be utilized to determine to the density of the wick region by Eq. (2), and the specific heat capacity is obtained according to Eq. (3).

$$\rho_{wick} = \varepsilon\rho_l + (1-\varepsilon)\rho_s \quad (2)$$

$$C_{wick} = [\varepsilon\rho_l C_l + (1-\varepsilon)\rho_s C_s] / \rho_{wick} \quad (3)$$

where r_{wick}, r_l, r_s are respectively the densities of the wick, working fluid and copper powder, C_{wick}, C_l, C_s are respectively the specific heat capacity of the wick, working fluid and copper powder, and ε is the porosity.

2.2.3. Vapor Core

ISSN 2616-5767 Vol.3, Issue 6: 199-208, DOI: 10.25236/AJETS.2020.030620

The vapor flow was considered incompressible, laminar and fully developed. By assuming the relationship between pressure drop and temperature drop in accordance with the Clapeyron equation and the ideal gas law[17, 18], the effective thermal conductivity of the vapor core in a tubular heat pipe can be calculated by Eq.(4) [17].

$$k_{vapor} = \frac{r_v^2 L^2 \rho P_v}{8\mu R T^2} \tag{4}$$

where r_v is the cross-section radius of the vapor core. L is the latent heat of working fluid. ρ, P_v, μ, R and T is respectively the density, the saturation pressure, the dynamic viscosity, the gas constant per unit mass and the temperature of the water vapor. The k_{vapor} was calculated as $4.69\times10^{6} Wm^{-1}K^{-1}$ using the properties of saturated water vapor at a temperature of 40 ℃.

2.3 Thermal Model of the Battery

The lithium ion battery is simplified to an anisotropic cuboid, and the thermal conductivity of the vertical stacking direction of the vertical cell is smaller than the thermal conductivity of the parallel direction. The properties of the heat pipe and the battery, including the specific heat capacity, thermal conductivity density, were listed in Table 1.

It is assumed that during the entire operation process, the heat generation rate of the battery is a constant value which is regarded as the maximum power during the highest sustainable constant-current discharge rate. In the present research, the heat generation rate is in the range of 20-80 W per cell.

2.4 Numerical Procedures

In this calculation, numerical studies were performed by the commercial CFD software-ANSYS Workbench 17.2 FLUENT using a parallel solver in a double precision mode. Heat radiation transfer is negligible and was not considered.

Cartesian grids were employed to realize the spatial discretization of the domain models. Denser girds were applied in the non-slip boundary regions where the flow and temperature gradients are greater, i.e., the area around heat pipes and the heat transfer interface of the battery. The grid independent test was performed by gradually refining the mesh size (in this study, three different meshes containing 2628477, 4737970 and 7895174 cells, respectively) to ensure that the mesh size has little impact on the results. The control parameter for grid independent test was the maximum temperature of the heat transfer interface of the battery. According to the procedure described [19], the grid convergence index (GCI) was 2.81%. Fig. 2 shows the mesh used in this numerical investigation.

ISSN 2616-5767 Vol.3, Issue 6: 199-208, DOI: 10.25236/AJETS.2020.030620

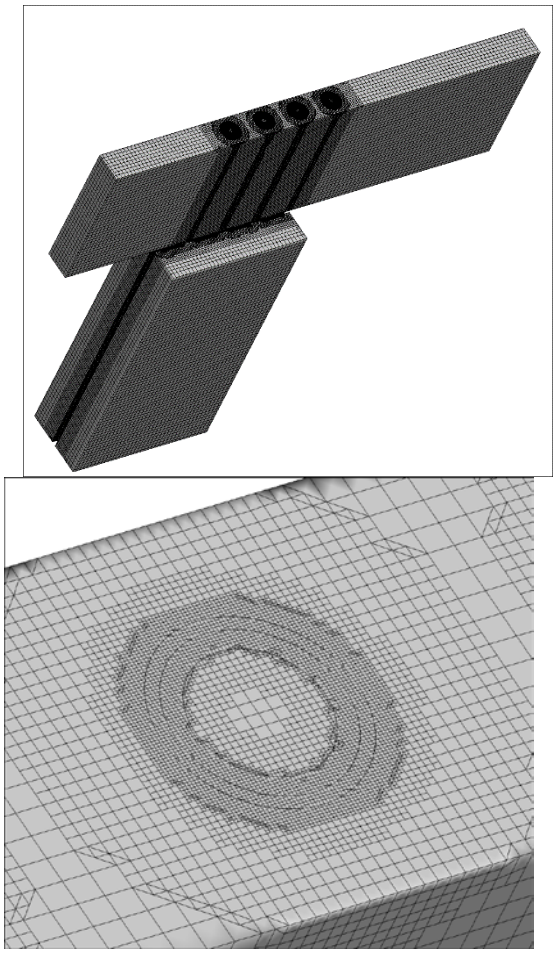

Fig.2 The Hexahedral Mesh Used in the Present Numerical Study

3. Effects of Coolant Flow Rate and Coolant Inlet Temperature

In this section, the effect of the coolant flow rate and coolant inlet temperature of the heat pipe cooling system on the temperature of the battery surface is discussed. The maximum temperature (T_{max}) of battery surface with different coolant flow rates and inlet temperatures under different input powers processes is shown in Fig. 3. The cooling flow rate for studied ranges from 1 L/min to 3 L/min, and the inlet temperature ranges from 15℃ to 35℃. The input power changes every 600 s from 20 W to 50 W while in each period it keep a constant value. The initial temperature of the cooling system and the battery is the same as the coolant inlet temperature in each condition.

ISSN 2616-5767 Vol.3, Issue 6: 199-208, DOI: 10.25236/AJETS.2020.030620

As Fig. 3 illustrated, T_{max} increased with the input power and coolant inlet temperature and decreased with the increasing coolant flow rate. However while the flow rate increasing, the reduction of T_{max} gradually decreased. The temperature difference of the battery surface △T also increased with the input power and decreased with the increasing coolant flow rate. It is worth noting that the temperature difference hardly changes with coolant inlet temperature.

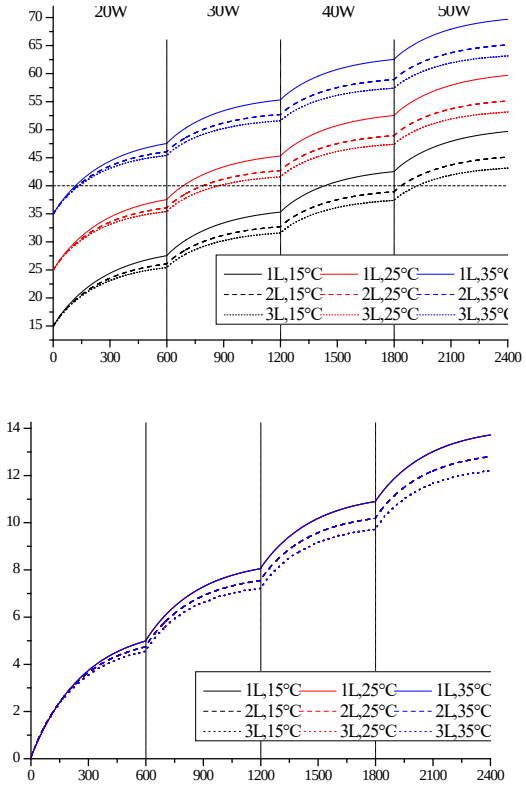

Fig.3 Temperature Response of Battery (a) T_{max} and (B) △t with Different Coolant Flow Rates Underdifferent Coolant Inlet Temperature

Temperature response of battery at coolant flow rate $q_v = 2L/\min$ under different coolant inlet temperature is displayed in Fig. 4. According to Fig. 4(a), within the scope of this study T_{max} is always below 40 °C under $T_c = 15\ °C$ even at the heat generation rate of 50 W/cell. And T_{max} is also below 40 °C under

ISSN 2616-5767 Vol.3, Issue 6: 199-208, DOI: 10.25236/AJETS.2020.030620

$T_c = 25\ °C$ with heat generation rate less than 30 W/cell. And $T_{\max}$ exceed 40 °C even at the heat generation rate of 20 W/cell. As shown in Fig. 4(b), $\triangle T$ did not vary as temperature increase.

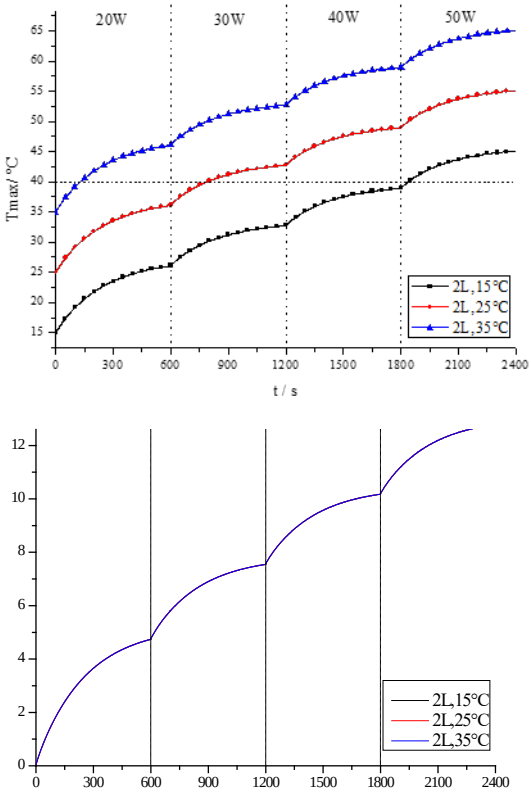

Fig.4 Temperature Response of Battery ($q_v = 2L/\min$): (a) $T_{\max}$ and $\triangle t$ Variation with Input Different Powers and Coolant Inlet Temperature

Fig.5 Displays the Equilibrium Temperature of Battery under Different Coolant Inlet Temperatures, Coolant Flow Rate and Different Input Power.

ISSN 2616-5767 Vol.3, Issue 6: 199-208, DOI: 10.25236/AJETS.2020.030620

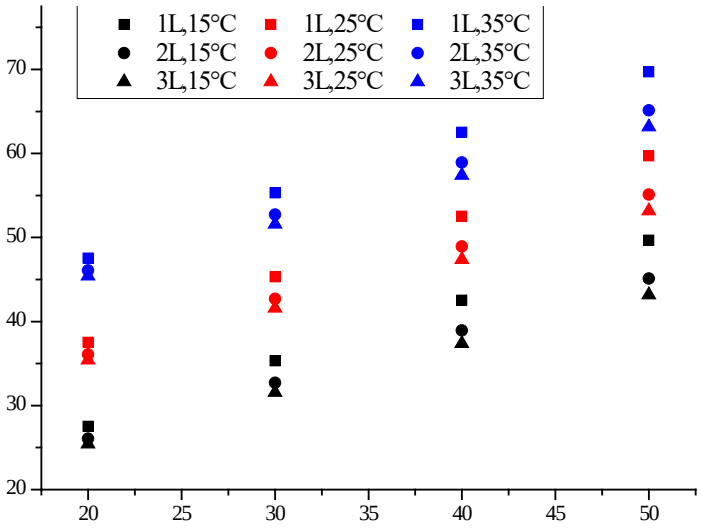

Fig.5 The Equilibrium T_{max} of Battery Surface under Different Coolant Inlet Temperatures, Coolant Flow Rate and Different Input Power

4. Conclusion

(1) T_{max} increased with the input power and coolant inlet temperature and decreased with the increasing coolant flow rate. However while the flow rate increasing, the reduction of T_{max} gradually decreased.

(2) The temperature difference of the battery surface △T also increased with the input power and decreased with the increasing coolant flow rate.

(3) Within the scope of this study T_{max} is always below 40 °C under $T_c = 15\ °C$, and is also below 40 °C under $T_c = 25\ °C$ with heat generation rate less than 30 W/cell.

Acknowledgments

Funding: This work was supported by the Natural Science Foundation of Jiangsu Province (Grants No. BK20170317).

ISSN 2616-5767 Vol.3, Issue 6: 199-208, DOI: 10.25236/AJETS.2020.030620

References

[1] CHOI Y S, KANG D M. Prediction of thermal behaviors of an air-cooled lithium-ion battery system for hybrid electric vehicles [J]. Journal of Power Sources, 2014, 270(2014): 273-280.
[2] ETACHERI V, MAROM R, ELAZARI R, et al. Challenges in the development of advanced Li-ion batteries: a review [J]. Energy & Environmental Science, 2011, 4(9): 3243-3262.
[3] TRAN T-H, HARMAND S, SAHUT B. Experimental investigation on heat pipe cooling for Hybrid Electric Vehicle and Electric Vehicle lithium-ion battery [J]. Journal of Power Sources, 2014, 265(2014): 262-272.
[4] RAO Z, WANG S, WU M, et al. Experimental investigation on thermal management of electric vehicle battery with heat pipe [J]. Energy Conversion and Management, 2013, 65(2013): 92-97.
[5] WALDMANN T, WILKA M, KASPER M, et al. Temperature dependent ageing mechanisms in Lithium-ion batteries–A Post-Mortem study [J]. Journal of Power Sources, 2014, 262(2014): 129-135.
[6] BANDHAUER T M, GARIMELLA S, FULLER T F. A critical review of thermal issues in lithium-ion batteries [J]. Journal of the Electrochemical Society, 2011, 158(3): R1-R25.
[7] TROXLER Y, WU B, MARINESCU M, et al. The effect of thermal gradients on the performance of lithium-ion batteries [J]. Journal of Power Sources, 2014, 247(2014): 1018-1025.
[8] WANG, TSENG K, ZHAO J, et al. Thermal investigation of lithium-ion battery module with different cell arrangement structures and forced air-cooling strategies [J]. Applied Energy, 2014, 134(2014): 229-238.
[9] GRECO A, CAO D, JIANG X, et al. A theoretical and computational study of lithium-ion battery thermal management for electric vehicles using heat pipes [J]. Journal of Power Sources, 2014, 257(2014): 344-355.
[10] RAO Z, HUO Y, LIU X. Experimental study of an OHP-cooled thermal management system for electric vehicle power battery [J]. Experimental Thermal and Fluid Science, 2014, 57(2014): 20-26.
[11] YE Y, SAW L H, SHI Y, et al. Numerical analyses on optimizing a heat pipe thermal management system for lithium-ion batteries during fast charging [J]. Applied Thermal Engineering, 2015, 86(2015): 281-291.
[12] YE Y, SAW L H, SHI Y, et al. Effect of thermal contact resistances on fast charging of large format lithium ion batteries [J]. Electrochimica Acta, 2014, 134(2014): 327-337.
[13] WANG, JIANG, XUE, et al. Experimental investigation on EV battery cooling and heating by heat pipes [J]. Applied Thermal Engineering, 2015, 88(2015): 54-60.
[14] YE Y, SHI Y, SAW L H, et al. Performance assessment and optimization of a heat pipe thermal management system for fast charging lithium ion battery packs [J]. International Journal of Heat and Mass Transfer, 2016, 92(2016): 893-903.
[15] ZUO Z, FAGHRI A. A network thermodynamic analysis of the heat pipe [J]. International Journal of Heat and Mass Transfer, 1998, 41(11): 1473-1484.

ISSN 2616-5767 Vol.3, Issue 6: 199-208, DOI: 10.25236/AJETS.2020.030620

[16] CHI S. Heat pipe theory and practice: a sourcebook [M]. 1976.
[17] PRASHER R S. A simplified conduction based modeling scheme for design sensitivity study of thermal solution utilizing heat pipe and vapor chamber technology [J]. Journal of Electronic Packaging, 2003, 125(3): 378-385.
[18] WEI X, SIKKA K. Modeling of vapor chamber as heat spreading devices; proceedings of the Thermal and Thermomechanical Proceedings 10th Intersociety Conference on Phenomena in Electronics Systems, 2006 ITHERM 2006, F, 2006 [C]. IEEE.
[19] CELIK I, GHIA U, ROACHE P, et al. Procedure for estimation and reporting of uncertainty due to discretization in CFD applications [J]. J Fluids Eng, 2008, 130(7): 078001.
[20] LIANG J, GAN Y, LI Y. Investigation on the thermal performance of a battery thermal management system using heat pipe under different ambient temperatures [J]. Energy Conversion and Management, 2018, 155(2018): 1-9.
[21] TIPPMANN S, WALPER D, BALBOA L, et al. Low-temperature charging of lithium-ion cells part I: Electrochemical modeling and experimental investigation of degradation behavior [J]. Journal of Power Sources, 2014, 252(305-316.
[22] PETZL M, KASPER M, DANZER M A. Lithium plating in a commercial lithium-ion battery–A low-temperature aging study [J]. Journal of Power Sources, 2015, 275(2015): 799-807.